Interactions of parametrically driven dark solitons. II. Néel-Bloch interactions

I. V. Barashenkov*
Department of Physics, University of Bayreuth, D-95440 Bayreuth, Germany

S. R. Woodford†
Theorie I, Institut für Festkörperforschung, Forschungszentrum Jülich, D-52428 Jülich, Germany
(Received 3 November 2006; published 9 February 2007)

The interaction between a Bloch and a Néel wall in the parametrically driven nonlinear Schrödinger equation is studied by following the dissociation of their unstable bound state. Mathematically, the analysis focuses on the splitting of a fourfold zero eigenvalue associated with a pair of infinitely separated Bloch and Néel walls. It is shown that a Bloch and a Néel wall interact as two classical particles, one with positive and the other one with negative mass.

DOI: 10.1103/PhysRevE.75.026605 PACS number(s): 05.45.Yv, 42.65.Tg

I. INTRODUCTION

In the preceding publication [1] we started our analysis of the interactions between dark solitons of the parametrically driven nonlinear Schrödinger (NLS) equation:

$$i\partial_T\Psi + \frac{1}{2}\partial_X^2\Psi + \Psi - |\Psi|^2\Psi = h\Psi^* - i\gamma\Psi. \qquad (1)$$

This equation arises in a wide variety of physical contexts; see [1] for references. In Eq. (1), h is the strength of the parametric driving and γ is the damping coefficient. In the nondissipative limit, when $\gamma=0$, the equation has two coexisting stable soliton solutions, the Bloch and the Néel wall. In [1], we considered forces existing between two Bloch walls and between two Néel walls. The present work completes the analysis by classifying the Néel-Bloch interactions. The understanding of this nonsymmetric situation requires a mathematical formalism different from the one used in [1]; this justifies the need for a separate treatment. Since the Bloch wall does not exist for $\gamma\neq 0$, we consider here the nondissipative case only. This is another distinction from Ref. [1].

Our analysis of the interaction between Bloch and Néel walls will be based on the study of linearized perturbations about their (unstable) bound state. Mathematically, this analysis reduces to the construction of eigenfunctions of a Schrödinger-like operator, acting in the space of vector-functions, with the potential consisting of two well-separated nonidentical potential wells. When the two wells are infinitely far apart, there are four zero eigenvalues in its spectrum, with two associated eigenfunctions. As the wells (produced by the Bloch and Néel walls) are moved closer together, the degeneracy is partially lifted, with only two eigenvalues remaining at the origin. The question here is whether the two nonzero eigenvalues move onto the imaginary axis—which would be the case of stability, or onto the real axis—in which case the bound state is unstable. We use matched asymptotic expansions to show that the second is the case and construct eigenfunctions associated with the two real eigenvalues.

The eigenfunction associated with the positive, unstable, eigenvalue contains the entire information on the character of interaction of two walls. We demonstrate that the outcome of the Néel-Bloch interaction depends on their left-right arrangement and the chirality of the Bloch wall. A Néel wall and a *right*-handed Bloch wall placed on its right will be moving in the same direction. If, however, we place a *left*-handed Bloch wall on the right of the Néel, the two walls will move in opposite directions—towards or away from each other, depending on the initial perturbation. The right-handed Bloch wall (on the left) and the Néel wall (on the right) will move in opposite directions, while a pair involving the left-handed Bloch on the left of the Néel, will move colinearly.

After the eigenfunctions associated with two opposite real eigenvalues have been constructed, the evolution of an arbitrary initial condition close to a pair of well-separated Bloch and Néel walls is not difficult to predict. Treating this initial condition as a perturbed Bloch-Néel bound state, its evolution will be determined by the projection of the perturbation on the bubble's unstable eigendirection. We illustrate this general approach by considering an example of initial condition in the form of a product of the Bloch and Néel wall.

Usually one tries to understand the interaction of solitons as interaction of pointlike particles; the particle description is physically appealing and mathematically lucid. We will show that a Bloch and a Néel wall *can* be treated as two classical particles. However, the interaction between these two particles is anomalous in the sense that the Bloch wall being attracted to the Néel wall does not necessarily imply the reciprocal attraction of the Néel to the Bloch. This anomaly can be understood by considering the Néel wall as a particle with negative mass. The "wrong" mass sign arises very naturally if one recalls what the Néel wall really is: a localized depression, a patch of low density moving over a high-density background. The only reason why this property was not fully appreciated before is because earlier studies focused

*On sabbatical leave from University of Cape Town. Permanent address: Department of Applied Mathematics, University of Cape Town, Rondebosch 7701, South Africa. Electronic address: Igor.Barashenkov@uct.ac.za; igor@odette.mth.uct.ac.za
†Electronic address: s.woodford@fz-juelich.de

on symmetric, Néel-Néel, interactions, which are, of course, nonanomalous.

The outline of this paper is as follows. In Sec. II we introduce *traveling* Bloch and Néel walls, and describe the Bloch-Néel bound state. Section III contains the main mathematical result of this paper, the asymptotic analysis of the splitting of the degenerate zero eigenvalue. In the next section (Sec. IV) we interpret the resulting eigenfunctions in terms of motions of the constituent walls. In Sec. V we describe how the eigenfunctions can be used to classify the interaction of a pair of Bloch and Néel walls and apply this approach to a characteristic example. Finally, the main results are summarized in Sec. VI where we also interpret the interaction of the walls as interaction of opposite mass-sign particles.

II. MOVING BLOCH AND NÉEL WALLS AND THE BLOCH-NÉEL COMPLEX

In this paper, we restrict ourselves to the undamped situation, $\gamma=0$. As in [1], we let

$$\Psi(X,T) = iA\,\psi(x,t), \quad x = AX, \quad t = A^2T, \tag{2}$$

with

$$A = \sqrt{1+h}. \tag{3}$$

Equation (1) becomes

$$i\psi_t + \frac{1}{2}\psi_{xx} - |\psi|^2\psi + \frac{1}{A^2}\psi + \frac{h}{A^2}\psi^* = 0. \tag{4}$$

This is the form of the parametrically driven NLS that will be used in this paper. The stable background solutions of Eq. (4) are $\psi_{\text{flat}}=\pm 1$. Without loss of generality we assume that $h>0$.

The two topological solitons of Eq. (4) were introduced in Ref. [1]. One is the Néel wall [2–6]:

$$\psi_N(x) = -\tanh(x). \tag{5}$$

Note that we are introducing the Néel wall differently from [1], with an extra negative sign in front of the tanh. This is done for later convenience. [In Ref. [1], we would refer to the solution (5) as an *antiwall*.]

The second topological soliton is the Bloch wall [4,5,7,8]:

$$\psi_B(x) = \tanh(Bx) \pm i\sqrt{1-B^2}\,\operatorname{sech}(Bx), \tag{6}$$

where

$$B = 2\frac{\sqrt{A^2-1}}{A} = 2\sqrt{\frac{h}{1+h}}.$$

Equation (6) with the positive sign in front of the imaginary part describes the right-handed Bloch wall while in the case of the negative sign, the wall is said to be left-handed (see [1] for details).

The Néel wall exists for all $h>0$ whereas the Bloch wall exists only for $A^2<\frac{4}{3}$, i.e., for $0<h<\frac{1}{3}$. Since we are interested in the Bloch-Néel interaction, the latter will be our region of consideration. Both the Bloch and Néel walls are stable in their entire regions of existence, $0<h<\frac{1}{3}$ and $h>0$, respectively [9].

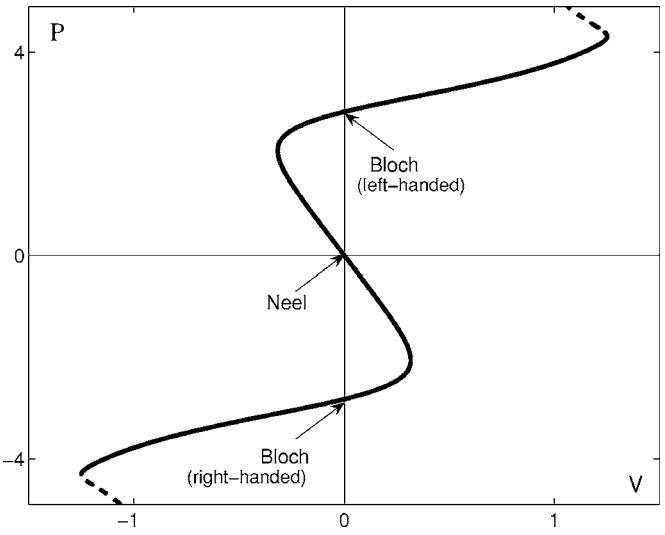

FIG. 1. The bifurcation diagram for the stationary and traveling Bloch and Néel walls with $h<\frac{1}{3}$ (adapted from Ref. [9]). The momentum (8) is used as the bifurcation measure. The solid curve indicates stable and dashed curve unstable solutions. Note that the mass of the Néel wall (defined as dP/dv) is opposite to the mass of the Bloch wall. In this plot, $h=0.05$.

The Bloch and Néel walls can be continued to nonzero velocity for all h values for which they exist [9]. The moving walls of the form $\psi=\psi(x-vt)$ are found as solutions of the ordinary differential equation

$$-iv\psi_x + \frac{1}{2}\psi_{xx} - |\psi|^2\psi + \frac{1}{A^2}\psi + \frac{h}{A^2}\psi^* = 0. \tag{7}$$

The solution obtained by the continuation from the stationary Néel wall $\psi_N(x)$ will be referred to as the "moving Néel wall" and denoted $\psi_N(v;x)$. In a similar way, the solution obtained by continuing $\psi_B(x)$ in v will be called the "moving Bloch wall"; to be denoted $\psi_B(v;x)$. The traveling walls are stable for all velocities v [9].

An important characteristic of solutions of Eq. (4) is their field momentum:

$$P = \frac{i}{2}\int (\psi\psi_x^* - \psi^*\psi_x)dx. \tag{8}$$

The momentum is conserved: $dP/dt=0$. When we take the complex conjugate of $\psi(x,t)$, the associated momentum changes its sign: $P[\psi^*]=-P[\psi]$. Consequently, the momenta of two stationary Bloch walls with opposite chiralities are opposite. The right-handed Bloch wall has negative momentum, while the left-handed wall's momentum is positive. The momentum of the stationary Néel wall is, naturally, equal to zero. Figure 1 shows the momenta of stationary and traveling Bloch and Néel walls. These will be denoted P_B and P_N, respectively:

$$P_B = P_B(v) \equiv P[\psi_B(v;x)], \tag{9a}$$

$$P_N = P_N(v) \equiv P[\psi_N(v;x)]. \tag{9b}$$

According to Fig. 1, when the right-handed Bloch wall is continued into the region $v>0$, it transforms into the moving Néel wall. In a similar way, when we path-follow the left-handed Bloch wall to large negative velocities, the corresponding branch turns into the branch of traveling Néel walls. Thus the classification of moving solutions into Bloch and Néel walls is only sensible for sufficiently small v; for higher velocities, there is no qualitative difference between the two types of walls.

One more observation with regard to Fig. 1 concerns particle properties of the two walls. While the stationary Bloch wall has positive mass, $m_B \equiv (dP_B/dv)_{v=0} > 0$, the mass of the Néel wall is negative: $m_N \equiv (dP_N/dv)_{v=0} < 0$. This property will be crucial for the particle interpretation of the Néel-Bloch interaction (Sec. VI).

In addition to the Bloch and Néel domain walls, Eq. (4) possesses nontopological solitons. One such solution, arising for $h=\frac{1}{15}$, is well-known [7,10–12]:

$$\psi = 1 - \frac{3}{2}\,\mathrm{sech}^2\left(\frac{x}{2}\right) \pm \frac{3i}{2}\tanh\left(\frac{x}{2}\right)\mathrm{sech}\left(\frac{x}{2}\right). \tag{10}$$

Recently, it has become clear that this solution is a member of a one-parameter family of solutions which exist for all $h<\frac{1}{3}$ [13]. For each h, this family has the following analytical expression:

$$\psi_b = \frac{p + i\sigma q}{\mathcal{D}}, \tag{11a}$$

where

$$p = 1 - e^{\phi_1+2\beta} - e^{2\phi_2+2\beta} + e^{\phi_1+2\phi_2}, \tag{11b}$$

$$q = 2(1+B)e^{\phi_2}(1 - e^{\phi_1}), \tag{11c}$$

and

$$\mathcal{D} = 1 + e^{\phi_1+2\beta} + e^{2\phi_2+2\beta} + e^{\phi_1+2\phi_2}. \tag{11d}$$

In Eq. (11), σ is a sign factor: $\sigma=\pm 1$; the exponents ϕ_1, ϕ_2 are

$$\phi_1 = 2(x+s), \quad \phi_2 = B(x-s),$$

and β is defined by

$$B \equiv \tanh\beta.$$

The solution Eq. (11) describes a bound state, or a complex, of a Bloch and a Néel wall, with the parameter s characterizing the distance between the centers of the two walls [13]. The choice $s>0$ corresponds to the Bloch wall on the right of the Néel wall; for $s<0$, the Bloch wall is on the left. The solution (10) corresponds to $s=0$ (and $h=1/15$). The sign factor σ determines the chirality of the Bloch wall bound in the complex: $\sigma=1$ implies that the Bloch wall is left-handed, while $\sigma=-1$ identifies a complex with a right-handed Bloch wall.

Equation (11) can also be interpreted as a bubble of one phase ($\psi=-1$) embedded in a background of a different phase ($\psi=1$); we will frequently be referring to this solution as a "bubble" [14].

The analysis of the bound state Eq. (11) will provide the understanding of the Bloch-Néel interaction.

III. SPLITTING OF THE DEGENERATE ZERO MODES

A. Stability problem for the complex

To study the stability of the bubble Eq. (11), as well as to explore the phase space in the neighborhood of this solution, we linearize Eq. (4) in the small perturbation $\delta\psi(x,t)$. Assuming the time dependence of the form $\delta\psi(x,t)=[u(x)+iw(x)]e^{\lambda t}$ results in the eigenvalue problem

$$\mathcal{H}\vec{\varphi} = \lambda J\vec{\varphi}, \tag{12}$$

where $\vec{\varphi}$ is a 2-vector made of the real and imaginary parts of the perturbation:

$$\vec{\varphi} = \begin{pmatrix} u \\ w \end{pmatrix},$$

J is a skew-symmetric matrix

$$J = \begin{pmatrix} 0 & -1 \\ 1 & 0 \end{pmatrix}, \tag{13}$$

and $\mathcal{H}$ is a Hermitian operator:

$$\mathcal{H} = -\frac{I}{2}\partial_x^2 + \begin{pmatrix} 3\mathcal{R}^2 + \mathcal{I}^2 - 1 & 2\mathcal{R}\mathcal{I} \\ 2\mathcal{R}\mathcal{I} & \mathcal{R}^2 + 3\mathcal{I}^2 - \dfrac{2-A^2}{A^2} \end{pmatrix}. \tag{14}$$

In the last equation, I stands for the 2×2 identity matrix, and $\mathcal{R}$ and $\mathcal{I}$ are the real and imaginary parts of the solution Eq. (11): $\psi_b=\mathcal{R}(x)+i\mathcal{I}(x)$. In what follows, we restrict our attention to the bound state with the Néel wall on the left of the Bloch wall [$s>0$ in Eq. (11)]. The results for $s<0$ will be recovered by exploiting the symmetry $\psi(-x;-s)=\psi^*(x;s)$ of the solution Eq. (11). Since the dynamics described by Eq. (4) are invariant under the reflection $x\to -x$, the evolution of a bubble with $s=s_0<0$ will follow the same pattern as the evolution of the complex conjugate bubble with positive $s=-s_0$.

For all values of s, the continuous spectrum of the operator $\mathcal{H}$ lies on the imaginary axis, with $|\mathrm{Im}\,\lambda| > B$, and does not give rise to instabilities. For $s=\infty$, the separation of the Bloch and Néel wall in the bubble is infinite and so we have essentially two independent stationary (but potentially mobile) walls, each having two zero eigenvalues in its linearized spectrum. One of these stems from the translation invariance while the other one is associated with velocity boosts of the corresponding wall. For finite s, only two of the four zero eigenvalues remain in the spectrum: one pertaining to the translation invariance of the complex as a whole and the other one associated with variations of the interwall separation. In this section we compute, perturbatively, the arising

nonzero eigenvalues (and hence classify the stability of the bubble). We also construct the eigenfunctions associated with the real eigenvalues—these will provide insight into the evolution of the unstable bound state and nearby initial conditions.

The lifting of the degeneracy of a repeated eigenvalue of the scalar Schrödinger operator with the potential comprising two identical potential wells with large separation is discussed in the classical textbook [15]. This analysis is not helpful in our case, unfortunately, for three reasons: (i) our $\mathcal{H}$ operates on vector, not scalar, functions; (ii) the potential wells formed by the Bloch and Néel walls are not identical; and (iii) the analysis in [15] *postulates* a particular form of the wave function on symmetry grounds, rather than deriving it within some perturbation formalism—as a result, the generalization to the vector nonsymmetric case is not straightforward.

Our treatment will be based on expanding the eigenfunction in the asymptotic series near the cores of the two walls and matching the resulting expansions in the overlap region $x \sim 0$. This approach builds on the asymptotic procedure used for the study of the stability of the traveling dark soliton [16].

B. Left expansion

We will do all our calculations for the case $s>0$ (i.e., for the Bloch wall on the right of the Néel wall). Furthermore, we will restrict ourselves to the right-handed Bloch wall only ($\sigma=-1$). The other three possible combinations of σ and $\mathrm{sgn}(s)$ will be commented upon at the end of Sec. III.

First, let $x \in (-\infty, x_0)$, where $x_0>0$ is a fixed value independent of s (so that $x_0<s$). In this region the real and imaginary parts of the bubble solution Eq. (11) can be written as

$$\mathcal{R} = -\tanh\xi + \frac{\sinh[2(\xi-\beta)]}{\cosh^2\xi} e^{2B(\xi-2s-\beta)} + \cdots,$$

$$\mathcal{I} = 2(\tanh\xi - B) e^{B(\xi-2s-\beta)} + \cdots, \tag{15}$$

where

$$\xi \equiv x + s + \beta, \tag{16}$$

and we have dropped terms of order $e^{3B(\xi-2s-\beta)}$ and smaller. Equations (15) can be seen as expansions of two functions of ξ, defined for $-\infty<\xi<\infty$, in powers of $\varepsilon = e^{-2Bs}$. Accordingly, the operator $\mathcal{H}$ in Eq. (14) expands as

$$\mathcal{H} = \mathcal{H}_N + \varepsilon\mathcal{H}_N^{(1)} + \varepsilon^2\mathcal{H}_N^{(2)} + \cdots. \tag{17}$$

Here, $\mathcal{H}_N$ is the unperturbed linearized operator of the Néel wall centered at $\xi=0$, i.e., Eq. (14) with $\mathcal{R}=-\tanh\xi$ and $\mathcal{I}=0$. Guided by the results of (our own) numerical analysis, we *assume* that λ is of order ε:

$$\lambda = \lambda_0\varepsilon.$$

(As we will see, this asumption leads to a self-consistent perturbation scheme.) This implies that the eigenfunction $\vec{\varphi}$ in the eigenvalue problem (12) can also be expanded in powers of ε:

$$\vec{\varphi}(\xi) = a\vec{\psi}_N'(\xi) + \varepsilon\vec{\varphi}_1(\xi) + \varepsilon^2\vec{\varphi}_2(\xi) + \cdots. \tag{18}$$

Here $\vec{\psi}_N' \equiv \partial_\xi\vec{\psi}_N$, and $\vec{\psi}_N=(\mathcal{R}_N,\mathcal{I}_N)=(-\tanh\xi,0)$. The coefficient a is arbitrary at this stage [$a=O(1)$].

Substituting Eqs. (17)–(18) into Eq. (12) and equating coefficients of like powers of ε, yields, at order ε^1:

$$\mathcal{H}_N\vec{\varphi}_1 + a\mathcal{H}_N^{(1)}\vec{\psi}_N' = a\lambda_0 J\vec{\psi}_N'. \tag{19}$$

To solve Eq. (19), we note that $\dot{\vec{\psi}}_N$ is a generalized eigenvector associated with the zero eigenvalue:

$$\mathcal{H}_N\dot{\vec{\psi}}_N = -J\vec{\psi}_N'. \tag{20}$$

Here ψ_N is considered as a solution of the form $\psi=\psi(x-vt)$ of Eq. (7), while the overdot indicates differentiation with respect to velocity v (and not time): $\dot{\vec{\psi}}_N \equiv (\partial_v\vec{\psi}_N)_{v=0}$. (This will be our convention until the end of Sec. III.) Also, we know that $\vec{\psi}_b' \equiv \partial_x\vec{\psi}_b$ and $\partial_s\vec{\psi}_b$ are zero modes of the perturbed operator (14) where $\vec{\psi}_b(x)=(\mathcal{R},\mathcal{I})$ is the bubble solution Eq. (11), and $-\infty<x<\infty$. Using Eq. (15), we write

$$\vec{\psi}_b' = \vec{\psi}_N' + \varepsilon(\vec{\chi}_1 + \vec{y}_1) + \varepsilon^2(\vec{\chi}_2 + \vec{y}_2) + \cdots,$$

$$\partial_s\vec{\psi}_b = \vec{\psi}_N' + \varepsilon(\vec{\chi}_1 - \vec{y}_1) + \varepsilon^2(\vec{\chi}_2 - \vec{y}_2) + \cdots, \tag{21}$$

where

$$\vec{\chi}_1(\xi) = 2e^{B(\xi-\beta)}\,\mathrm{sech}^2\xi \begin{pmatrix} 0 \\ 1 \end{pmatrix}, \tag{22}$$

$$\vec{y}_1(\xi) = 2Be^{B(\xi-\beta)}(\tanh\xi - B)\begin{pmatrix} 0 \\ 1 \end{pmatrix}, \tag{23}$$

$$\vec{\chi}_2(\xi) = e^{2B(\xi-\beta)}\frac{d}{d\xi}\frac{\sinh[2(\xi-\beta)]}{\cosh^2\xi}\begin{pmatrix} 1 \\ 0 \end{pmatrix}, \tag{24}$$

$$\vec{y}_2(\xi) = 2Be^{2B(\xi-\beta)}\frac{\sinh[2(\xi-\beta)]}{\cosh^2\xi}\begin{pmatrix} 1 \\ 0 \end{pmatrix}. \tag{25}$$

Substituting expansions (17) and (21) into $\mathcal{H}\vec{\psi}_b' = \mathcal{H}\partial_s\vec{\psi}_b = 0$, the order ε^1 gives a useful identity:

$$\mathcal{H}_N\vec{\chi}_1 + \mathcal{H}_N^{(1)}\vec{\psi}_N' = 0; \tag{26}$$

we also note that

$$\mathcal{H}_N\vec{y}_1 = 0. \tag{27}$$

Using Eqs. (20) and (26), we can solve Eq. (19) in the class of functions bounded as $|\xi| \to \infty$:

$$\vec{\varphi}_1(\xi) = -a\lambda_0\dot{\vec{\psi}}_N + a\vec{\chi}_1.$$

The emerging vector-function $\vec{\varphi}=a\vec{\psi}_N'+\varepsilon\vec{\varphi}_1+\cdots$ decays, exponentially, both as $\xi\to-\infty$ and $\xi\to+\infty$ and hence it is intuitively clear that it *cannot* describe the behavior of the eigenfunction of the bound state in the region under consid-

eration ($x<0$). Indeed, the eigenfunction should include a term growing as $\xi\to+\infty$ and representing the tail of the Bloch wall situated in the region $x>0$. Therefore we need to add to $\vec{\varphi}$ a solution of the equation $\mathcal{H}_N\vec{y}=0$ which decays as $\xi\to-\infty$ but grows as $\xi\to\infty$. This solution is already available [see Eq. (27)]; it is given just by Eq. (23). Note that the other two linearly independent solutions of equation $\mathcal{H}_N\vec{y}=0$ (other than $\vec{\psi}_N'$ and $\vec{y}_1$) are growing as $\xi\to-\infty$; these are clearly not acceptable for our purposes.

Finally, the full order-ε^1 perturbation is $-a\lambda\dot{\vec{\psi}}_N+a\varepsilon\vec{\chi}_1+C_1\vec{y}_1$, and the eigenfunction $\vec{\varphi}$ becomes, in the region $x<x_0$ ("left region"):

$$\vec{\varphi}(\xi)=a\vec{\psi}_N'-a\lambda\dot{\vec{\psi}}_N+a\varepsilon\vec{\chi}_1+C_1\vec{y}_1+O(\varepsilon^2), \tag{28}$$

with $\vec{y}_1$ as in Eq. (23) and the constant C_1 to be found from the matching condition at a later stage. (Here we are implicitly assuming that this constant will be of order ε. If, however, it is of order ε^2 or higher, the term $C\vec{y}_1$ will only appear at higher orders of the expansion.)

C. Right expansion

Now let $x\in(-x_0,\infty)$. (We remind that $x_0>0$ is a fixed value independent of s; $x_0<s$.) Here, the real and imaginary parts of the bubble are given by

$$\mathcal{R}=\tanh(B\eta-\beta)-\frac{\sinh(2B\eta)}{\cosh^2(B\eta-\beta)}e^{-2(\eta+2s)}+\cdots,$$

$$\mathcal{I}=\frac{\operatorname{sech}\beta}{\cosh(B\eta-\beta)}-\frac{2\cosh(B\eta)}{\cosh^2(B\eta-\beta)}e^{-2(\eta+2s)}+\cdots, \tag{29}$$

where

$$\eta\equiv x-s \tag{30}$$

and we have dropped terms of order $e^{-4(\eta+2s)}$. Equations (29) can be seen as expansions of the functions $\mathcal{R}(\eta)$ and $\mathcal{I}(\eta)$ (with $-\infty<\eta<\infty$) in powers of $\mu=e^{-4s}$. Accordingly, the operator $\mathcal{H}$ expands as

$$\mathcal{H}=\mathcal{H}_B+\mu\mathcal{H}_B^{(1)}+\mu^2\mathcal{H}_B^{(2)}+\cdots. \tag{31}$$

Here, $\mathcal{H}_B$ is the unperturbed linearized operator of the Bloch wall centered at $\eta=\beta/B$, Eq. (14) with $\mathcal{R}_B=\tanh(B\eta-\beta)$ and $\mathcal{I}_B=\operatorname{sech}\beta\operatorname{sech}(B\eta-\beta)$. Note that the expansion parameter μ is, in general, incommensurate with ε and hence it is not *a priori* obvious what the expansion of the eigenfunction $\vec{\varphi}(\eta)$ will be. Letting $\vec{\varphi}(\eta)=\vec{\psi}_B'+\hat{\vec{\varphi}}$, where $\hat{\vec{\varphi}}$ has *some* order of smallness, and substituting into Eq. (12), we get

$$\mathcal{H}_B\hat{\vec{\varphi}}=\lambda_0\varepsilon J\vec{\psi}_B', \tag{32}$$

where we have dropped terms of order μ because μ is smaller than ε (and even ε^2). From Eq. (32) it is clear that the leading-order correction to the translation mode of the free-standing Bloch wall is of order ε (and not μ or $\mu^{1/2}$ as one might have been tempted to think).

Recalling that $\dot{\vec{\psi}}_B(\eta)\equiv(\partial_v\vec{\psi}_B)_{v=0}$ is a generalized eigenvector associated with the zero eigenvalue of the free-standing Bloch wall:

$$\mathcal{H}_B\dot{\vec{\psi}}_B=-J\vec{\psi}_B',$$

the localized solution of Eq. (32) is given by $\hat{\vec{\varphi}}=-\lambda\dot{\vec{\psi}}_B$, and so (the localized part of) the eigenfunction $\vec{\varphi}$ can be written as

$$\vec{\varphi}(\eta)=b\vec{\psi}_B'-\lambda b\dot{\vec{\psi}}_B+O(\varepsilon^2,\mu), \tag{33}$$

where b is an arbitrary constant of order 1.

The eigenfunction (33) decays, exponentially, as $\eta\to-\infty$ and therefore cannot represent the $(x>0)$-behavior of the eigenfunction of the bound state. (For there is no connection of such an eigenfunction to the region $x<0$ where the Néel wall is located.) In order to obtain the correct behavior, we need to add a solution of equation $\mathcal{H}_B\vec{z}=0$ which decays as $\eta\to+\infty$ but grows as $\eta\to-\infty$. The equation has only two solutions that decay as $\eta\to\infty$; one is the translation mode

$$\vec{\psi}_B'=(\mathcal{R}_B',\mathcal{I}_B')=\left(B\operatorname{sech}^2(B\eta-\beta),\ -B\operatorname{sech}\beta\frac{\tanh(B\eta-\beta)}{\cosh(B\eta-\beta)}\right), \tag{34}$$

and the other one can be found by expanding the exact null eigenfunctions of the bubble, $\vec{\psi}_b'\equiv\partial_x\vec{\psi}_b$ and $\partial_s\vec{\psi}_b$, in powers of μ (in the region $x>-x_0$). We have

$$\vec{\psi}_b'=\vec{\psi}_B'+\mu(\vec{z}_1-\vec{\theta}_1)+O(\mu^2),$$

$$\partial_s\vec{\psi}_b=-\vec{\psi}_B'+\mu(\vec{z}_1+\vec{\theta}_1)+O(\mu^2), \tag{35}$$

where

$$\vec{z}_1(\eta)=\frac{2e^{-2\eta}}{\cosh^2(B\eta-\beta)}\begin{pmatrix}\sinh(2B\eta)\\ 2\cosh(B\eta)\end{pmatrix} \tag{36}$$

and

$$\vec{\theta}_1(\eta)=\frac{e^{-2\eta}}{2}\frac{d}{d\eta}(e^{2\eta}\vec{z}_1). \tag{37}$$

Substituting Eqs. (31) and (35) into $\mathcal{H}\vec{\psi}_b'=\mathcal{H}\partial_s\vec{\psi}_b=0$, we obtain $\mathcal{H}_B\vec{z}_1=0$ which means that Eq. (36) gives exactly the solution we are looking for.

Finally, the correct behavior of the eigenfunction $\vec{\varphi}$ in the region $x>-x_0$ (the "right" region) is given by

$$\vec{\varphi}(\eta)=b\vec{\psi}_B'-\lambda b\dot{\vec{\psi}}_B+D\vec{z}_1+O(\varepsilon^2), \tag{38}$$

where $\vec{z}_1$ is given by Eq. (36) and the constant D is to be fixed later.

D. Asymptotic matching

Equations (28) and (38) give the leading terms in the asymptotic expansion of the eigenfunction $\vec{\varphi}$ in the regions

$x<x_0$ and $x>-x_0$, respectively. Before proceeding to the next order of the expansion (which will give us the eigenvalue λ), we need to make sure that the two expansions match in the overlap region $-x_0<x<x_0$.

In what follows, we will need the asymptotic behaviors of the generalized eigenvectors $\dot{\vec{\psi}}_N$ and $\dot{\vec{\psi}}_B$. The solution $\dot{\vec{\psi}}_N$ of Eq. (20) can be constructed in quadratures. The $|\xi|\to\infty$ asymptotic behavior is straightforward from the quadrature:

$$\dot{\vec{\psi}}_N(\xi) \to -\rho(B+1)e^{-B|\xi|}\begin{pmatrix}0\\1\end{pmatrix}, \tag{39}$$

where the factor

$$\rho = \frac{1}{B(1-B^2)}\int_{-\infty}^{\infty} \operatorname{sech}^2\xi\,(B-\tanh\xi)\,e^{B\xi}\,d\xi$$
$$= \frac{1}{1-B^2}\frac{\pi B/2}{\sin(\pi B/2)} > 0. \tag{40}$$

The $\eta\to\pm\infty$ asymptotics of the solution $\dot{\vec{\psi}}_B$ of equation $\mathcal{H}_B\dot{\vec{\psi}}_B=-J\dot{\vec{\psi}}_B'$ are given by

$$\dot{\vec{\psi}}_B(\eta) \to \begin{pmatrix} u_\pm e^{-|B\eta-\beta|} \\ w_\pm e^{-2|B\eta-\beta|}\end{pmatrix}, \tag{41}$$

where the constants $u_\pm$ and $w_\pm$ are easily found by direct substitution:

$$u_\pm = \mp\frac{4B(1+B)e^{-\beta}}{4-B^2}, \quad w_\pm = \frac{8B}{4-B^2}.$$

Using Eq. (39), the $(\xi\to+\infty)$ asymptotic behavior of the expansion (28) is given by

$$\vec{\varphi} \to \begin{pmatrix} -4ae^{-2(x+s+\beta)} \\ 0\end{pmatrix} + a\lambda\begin{pmatrix} 0 \\ \rho(B+1)e^{-B(x+s+\beta)}\end{pmatrix}$$
$$+ 8a\varepsilon e^{B(x+s)}\begin{pmatrix} 0 \\ e^{-2(x+s+\beta)}\end{pmatrix} + C_1\begin{pmatrix} 0 \\ 2B(1-B)e^{B(x+s)}\end{pmatrix}, \tag{42}$$

where we have substituted $x+s+\beta$ for each ξ. The $(\eta\to-\infty)$ asymptotic behavior of the expansion (38) is

$$\vec{\varphi} \to b\begin{pmatrix} 4Be^{2B(x-s)-2\beta} \\ 2(1+B)e^{-\beta}Be^{B(x-s)-\beta}\end{pmatrix} - \lambda b\begin{pmatrix} u_- e^{B(x-s)-\beta} \\ v_- e^{2B(x-s)-2\beta}\end{pmatrix}$$
$$+ D\begin{pmatrix} -4e^{-2(x-s)-2\beta} \\ 8e^{(B-2)(x-s)-2\beta}\end{pmatrix}. \tag{43}$$

Here we have replaced each η with $x-s$.

Equating coefficients of the exponential e^{Bx} in the bottom rows of Eqs. (42) and (43) determines the constant C_1:

$$C_1 = b\varepsilon. \tag{44}$$

Equating coefficients of the exponential e^{-2x} in the top rows of Eqs. (42) and (43) and the exponential $e^{(B-2)x}$ in the bottom rows, fixes the constant D:

$$D = a\mu. \tag{45}$$

(Both top and bottom rows lead to equivalent equations, so only one parameter is fixed.) Since D turns out to be smaller than λ and even λ^2, we can drop the term $D\vec{z}_1$ from $\vec{\varphi}_1$ and $\vec{\varphi}_2$.

There is a term in Eq. (42) which does not have a matching partner in Eq. (43), and the other way around, there are terms in Eq. (43) which do not have counterparts in Eq. (42). Consider, first, the term proportional to e^{-Bx} in Eq. (42). This exponential does not have a partner in Eq. (43); however, we can add a matching term $-a\lambda\dot{\vec{\psi}}_N(\xi)$ with $\xi=\eta+2s+\beta$ to the expansion (38). This term will be of order e^{-4Bs} for $\eta\sim0$ and hence will arise only at the next, ε^2–, order of the expansion. In a similar way, the exponentials e^{Bx} in the top row and e^{2Bx} in the bottom row of Eq. (43) do not have counterparts in the expansion (42). This can be taken care of by adding the term $-b\lambda\dot{\vec{\psi}}_B(\eta)$ with $\eta=\xi-2s-\beta$ to Eq. (28). The top and bottom rows of this term will appear only at the order ε^2 and ε^3, respectively. Finally, the last unmatched exponential e^{2Bx} in the top row of Eq. (43) will acquire a matching partner if we add $\varepsilon^2\vec{y}_2$ to Eq. (28), where $\vec{y}_2(\xi)$ is given by Eq. (25).

E. Secular equation

To identify the constants a, b and the eigenvalue λ we proceed to the next order of the perturbation expansion. As before, we treat the regions $x<0$ and $x>0$ separately. For $-\infty<x<x_0$, the order ε^2 gives

$$\mathcal{H}_N\vec{\varphi}_2 + \mathcal{H}_N^{(1)}\vec{\varphi}_1 + a\mathcal{H}_N^{(2)}\vec{\psi}_N' = \lambda_0 J\vec{\varphi}_1, \tag{46}$$

where $\vec{\varphi}_1$ is as in Eq. (28). The solvability condition of Eq. (46) is

$$(\vec{\psi}_N', \mathcal{H}_N^{(1)}\vec{\varphi}_1) + a(\vec{\psi}_N', \mathcal{H}_N^{(2)}\vec{\psi}_N') = \lambda_0(\vec{\psi}_N', J\vec{\varphi}_1), \tag{47}$$

where $(,)$ stands for the L^2-scalar product of two vector-functions of ξ:

$$(\vec{f},\vec{g}) = \int_{-\infty}^{\infty}(f^1g^1 + f^2g^2)d\xi.$$

To obtain Eq. (47), we have made use of the identity $(\vec{\psi}_N', \mathcal{H}_N\vec{\varphi}_2)=(\vec{\varphi}_2, \mathcal{H}_N\vec{\psi}_N')$, and the fact that $\mathcal{H}_N\vec{\psi}_N'=0$. However, since $\vec{\varphi}_2$ should include terms which have exponential growth as $\xi\to+\infty$, the validity of this identity [and hence of Eq. (47)] may be under suspicion. To reassure that the solvability condition is indeed correct, we note that the second-order perturbation should have the form

$$\varepsilon^2\vec{\varphi}_2(\xi) = -b\lambda\dot{\vec{\psi}}_B + \varepsilon^2\vec{y}_2 + C_2\vec{y}_1 + \varepsilon^2\tilde{\vec{\varphi}}_2, \tag{48}$$

where C_2 is a constant of order ε^2, and the function $\tilde{\vec{\varphi}}_2$ is bounded as $|\xi|\to\infty$. Note that the growing terms on the right-hand side of Eq. (48) (the first, second, and third terms) grow no faster than $e^{2B\xi}$ whereas $\vec{\psi}_N'$ decays as $e^{-2\xi}$ when $\xi\to+\infty$. Therefore, when doing each of the integrals $(\vec{\psi}_N', \mathcal{H}_N\dot{\vec{\psi}}_B)$, $(\vec{\psi}_N', \mathcal{H}_N\vec{y}_2)$, and $(\vec{\psi}_N', \mathcal{H}_N\vec{y}_1)$ by parts, the bound-

ary terms vanish. Consequently, we have $(\vec{\psi}'_N, \mathcal{H}_N\vec{\varphi}_2) = (\vec{\varphi}_2, \mathcal{H}_N\vec{\psi}'_N)$; Q.E.D.

Equation (47) can be simplified considerably if we use the identities arising at the order ε^2 of equations $\mathcal{H}\vec{\psi}'=0$ and $\mathcal{H}\partial_s\vec{\psi}=0$ with $\mathcal{H}$ expanded as in Eq. (17) and $\vec{\psi}'$, $\partial_s\vec{\psi}$ as in Eq. (21):

$$\mathcal{H}_N^{(2)}\vec{\psi}'_N + \mathcal{H}_N^{(1)}\vec{\chi}_1 + \mathcal{H}_N\vec{\chi}_2 = 0,$$

$$\mathcal{H}_N^{(1)}\vec{y}_1 + \mathcal{H}_N\vec{y}_2 = 0.$$

Taking the scalar product with $\vec{\psi}'_N$, these become

$$(\vec{\psi}'_N, \mathcal{H}_N^{(2)}\vec{\psi}'_N) + (\vec{\psi}'_N, \mathcal{H}_N^{(1)}\vec{\chi}_1) = 0,$$

$$(\vec{\psi}'_N, \mathcal{H}_N^{(1)}\vec{y}_1) = 0. \tag{49}$$

Using Eqs. (26), (44), and (49), Eq. (47) simplifies to

$$a\lambda^2(\vec{\psi}'_N, J\dot{\vec{\psi}}_N) - b\varepsilon\lambda(\vec{\psi}'_N, J\vec{y}_1) = 0. \tag{50}$$

Noting that $(\vec{\psi}'_N, J\dot{\vec{\psi}}_N) = (1/2)\dot{P}_N$ and evaluating the integral $(\vec{\psi}'_N, J\vec{y}_1)$, Eq. (50) becomes, finally,

$$\frac{\lambda^2}{2}\dot{P}_N\, a + 2\varepsilon\lambda\rho B^2(1-B^2)e^{-B\beta}b = 0. \tag{51}$$

Here P_N is the momentum of the Néel wall, Eq. (9b).

Turning to the region $-x_0 < x < \infty$, the eigenfunction has the expansion

$$\vec{\varphi}(\eta) = b\vec{\psi}'_B - \lambda b\dot{\vec{\psi}}_B + \varepsilon^2\vec{\varphi}_2 + O(\lambda^3, \mu), \tag{52}$$

where $\vec{\varphi}_2$ consists of a bounded part $\tilde{\vec{\varphi}}_2$ and a part that grows as $\eta \to -\infty$:

$$\varepsilon^2\vec{\varphi}_2(\eta) = \lambda^2\tilde{\vec{\varphi}}_2 - \lambda a\dot{\vec{\psi}}_N(\xi). \tag{53}$$

The order λ^2 of the expansion of $\mathcal{H}\vec{\varphi} = \lambda J\vec{\varphi}$ gives

$$\mathcal{H}_B(\lambda^2\tilde{\vec{\varphi}}_2 - a\lambda\dot{\vec{\psi}}_N) = -\lambda^2 bJ\dot{\vec{\psi}}_B. \tag{54}$$

The solvability condition is

$$-a\lambda(\vec{\psi}'_B, \mathcal{H}_B\dot{\vec{\psi}}_N) = -\lambda^2 b(\vec{\psi}'_B, J\dot{\vec{\psi}}_B), \tag{55}$$

where, this time,

$$(\vec{f}, \vec{g}) \equiv \int_{-\infty}^{\infty} (f^1 g^1 + f^2 g^2)\, d\eta.$$

At first glance, the scalar product on the left-hand side of Eq. (55) is zero as $\mathcal{H}_B\vec{\psi}'_B = 0$. However, $\dot{\vec{\psi}}_N$ grows as $\eta \to -\infty$: $\dot{\vec{\psi}}_N \sim e^{-B\eta}$, while $\vec{\psi}'_B$ does not decay fast enough—in fact, it decays at exactly the same rate: $\vec{\psi}'_B \sim e^{B\eta}$. Therefore $(\vec{\psi}'_B, \mathcal{H}_B\dot{\vec{\psi}}_N) \neq (\dot{\vec{\psi}}_N, \mathcal{H}_B\vec{\psi}'_B)$. [Note the difference from our analysis of the neighborhood of the Néel wall where $\vec{\psi}'_N$ decayed faster than the exponentially growing terms in $\vec{\varphi}_2$ would grow, and hence $(\vec{\psi}'_N, \mathcal{H}_N\vec{\varphi}_2) = (\vec{\varphi}_2, \mathcal{H}_N\vec{\psi}'_N)$ was indeed true.] Making use of the asymptotic expression (39) and taking care of the boundary term, we get, instead:

$$(\vec{\psi}'_B, \mathcal{H}_B\dot{\vec{\psi}}_N) = 2\varepsilon\rho B^2(1-B^2)e^{-B\beta}. \tag{56}$$

Finally, Eq. (55) becomes

$$-2\varepsilon\lambda\rho B^2(1-B^2)e^{-B\beta}a + \frac{\lambda^2}{2}\dot{P}_B b = 0, \tag{57}$$

where P_B is the momentum of the Bloch wall, Eq. (9a).

Equations (51) and (57) constitute a system of two linear equations for two unknowns, a and b. The associated characteristic equation is fourth-order in λ:

$$\lambda^2 \begin{vmatrix} \lambda\dot{P}_N & 4\varepsilon\rho B^2(1-B^2)e^{-B\beta} \\ 4\varepsilon\rho B^2(1-B^2)e^{-B\beta} & -\lambda\dot{P}_B \end{vmatrix} = 0.$$

The equation has two zero roots corresponding to the translation symmetry of the bound state as a whole and variations of the interwall separation; there is also a pair of real roots of opposite sign. Using Eq. (40), these are found to be

$$\lambda = \pm 2\pi \frac{B^3 e^{-B\beta}}{\sin(\pi B/2)} \frac{1}{\sqrt{-\dot{P}_N\dot{P}_B}} e^{-2Bs}. \tag{58}$$

(Note that $\dot{P}_N$ and $\dot{P}_B$ are opposite in sign—see Fig. 1; hence we have a positive quantity under the square root.) This is the first result of our analysis. The second result is the relation between a and b, the coefficients of the leading terms in the expansion of $\vec{\varphi}$:

$$\frac{a}{b} = \pm\sqrt{-\frac{\dot{P}_B}{\dot{P}_N}}. \tag{59}$$

Here the plus corresponds to the positive eigenvalue and minus to the negative one. (That is, the "unstable" eigenfunction has a and b of the same sign, both positive or negative, whereas the "stable" eigenfunction has the coefficients of the opposite sign; see Fig. 3(a,b) below.) In what follows it will be convenient to choose the normalization such that $a = \sqrt{\dot{P}_B} > 0$ for either sign of λ, while $b = \sqrt{-\dot{P}_N} > 0$ for $\lambda > 0$ and $b = -\sqrt{-\dot{P}_N} < 0$ for $\lambda < 0$. Thus the normalized eigenfunctions are

$$\vec{\varphi}_u = \sqrt{\dot{P}_B}(\vec{\psi}'_N - |\lambda|\dot{\vec{\psi}}_N + \varepsilon\vec{\chi}_1) + \sqrt{-\dot{P}_N}\varepsilon\vec{y}_1 + O(\varepsilon^2),$$

$$\vec{\varphi}_s = \sqrt{\dot{P}_B}(\vec{\psi}'_N + |\lambda|\dot{\vec{\psi}}_N + \varepsilon\vec{\chi}_1) - \sqrt{-\dot{P}_N}\varepsilon\vec{y}_1 + O(\varepsilon^2) \tag{60a}$$

for $x < 0$, and

$$\vec{\varphi}_u = \sqrt{-\dot{P}_N}(\vec{\psi}'_B - |\lambda|\dot{\vec{\psi}}_B) + O(\varepsilon^2),$$

$$\vec{\varphi}_s = -\sqrt{-\dot{P}_N}(\vec{\psi}_B' + |\lambda|\dot{\vec{\psi}}_B) + O(\varepsilon^2) \qquad (60b)$$

for $x>0$. Here $\vec{\varphi}_u$ and $\vec{\varphi}_s$ are the eigenfunctions associated with the positive and negative eigenvalue, respectively.

We conclude our calculation by commenting on the case of the complex involving a *left*-handed Bloch wall ($\sigma=+1$) and on the situation where the Bloch wall (right- or left-handed) is on the left of the Néel wall (i.e., $s<0$). These cases do not require a separate treatment. Indeed, let $(u(x),w(x))$ be the eigenvector associated with the eigenvalue λ (positive or negative) of the bubble Eq. (11) with $s>0$ and $\sigma=-1$. Changing $\sigma\to-\sigma$ changes the sign of the off-diagonal entries of the matrix (14); hence the vector $(u(x),-w(x))$ will give the eigenfunction associated with the eigenvalue $-\lambda$ for the bubble with $\sigma=1$. Therefore, the "unstable" eigenvector for the bubble with $s>0$ and $\sigma=+1$ is obtained from the "stable" eigenvector of the bubble with $s>0$ and $\sigma=-1$, just by changing the sign of its second component [compare Figs. 3(b) and 3(c) below]. To find the eigenfunctions for the Bloch wall on the left of the Néel, we note a symmetry of the bubble solution Eq. (11): $\psi_b(x,-s)=\psi_b^*(-x,s)$. According to this symmetry, changing $s\to-s$ in Eq. (11) is equivalent to replacing $x\to-x$ and taking the complex conjugate. Consequently, the vector $(u(-x),-w(-x))$ will serve as the eigenfunction associated with the eigenvalue $-\lambda$ for the bubble with $\sigma=-1$ and $s<0$. Finally, $(u(-x),w(-x))$ and λ are the eigenvector and the associated eigenvalue pertaining to the situation with $\sigma=+1$, $s<0$.

F. Numerical verification

The above perturbation results were verified numerically. (We used Fourier expansions of $\vec{\varphi}$ over 120 positive and 120 negative harmonics, on the interval $[-40,40]$.) In agreement with our expectations, for $s=\infty$ we have found four zero eigenvalues. Two of these remain at zero as s is decreased from infinity. The other two zero eigenvalues move to the real axis; one becomes positive and the other negative (Fig. 2). Their magnitudes are equal. This is a general property of linearizations of Hamiltonian systems of the form (12), with $\mathcal{H}$ Hermitian and J as in Eq. (13); it follows from the conservation of symplectic areas [17]. The eigenvalues return to zero as $s\to0$. These are the only eigenvalues with a nonzero real part in the spectrum of $\mathcal{H}$; hence for any finite, nonzero s, there is exactly one unstable mode. In addition, there are two pure imaginary eigenvalues detaching from the continuous spectrum as s decreases from infinity. These do not reach the origin; they remain on the imaginary axis and hence do not cause instability.

The structure of the numerical eigenfunctions $\vec{\varphi}_u$ and $\vec{\varphi}_s$ (shown in Fig. 3) is in exact agreement with Eqs. (59) and (60). The eigenfunctions transform (under $\sigma\to-\sigma, s\to-s$) exactly as predicted by the perturbation theory at the end of the preceding section.

In addition to the numerical solutions of the eigenvalue problem (12), we performed numerical simulations of the full time-dependent nonlinear Schrödinger equation (4). Simulations were carried out using a split-step pseudospectral method under periodic boundary conditions (see, e.g., [18]). Typically, we used an interval $(-L/2,L/2)$ with $L=60$, although for small h and large s (i.e., when the walls bound in the bubble are far apart and decay slowly to the background), $L=120$ was necessary. The time step was set at $\Delta t=2.5\times10^{-3}$. The code is stable for $\Delta t<\pi^{-1}(L/N)^2$, so for $L=120$ we were able to use $N=1024$ modes, while for $L=60$, we were limited to $N=512$. The spatial resolution $\Delta x=2\pi L/N$ was the same in both cases. Results of numerical

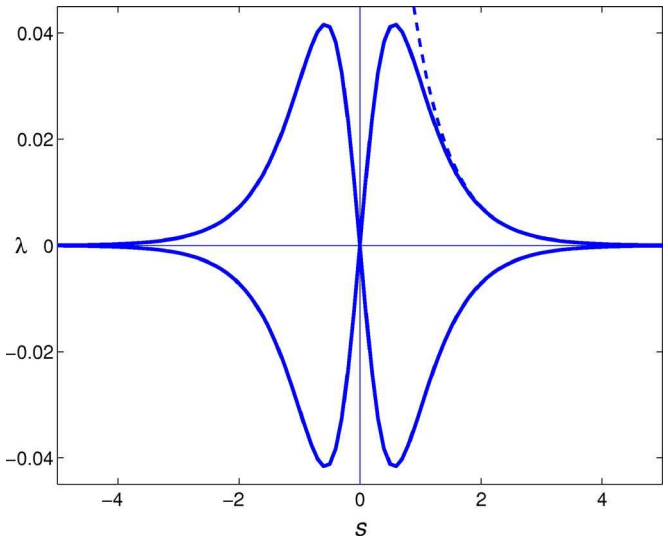

FIG. 2. (Color online) Two discrete real eigenvalues of the eigenvalue problem (12). The solid lines depict eigenvalues found numerically while the dashed line gives the perturbation approximation (58). This plot is for the case where the Bloch wall bound in the complex is right-handed; changing the chirality of the Bloch wall switches around the two branches, but leaves the overall shape the same. This figure pertains to $h=0.2$; for other h, the functions $\lambda(s)$ look similar.

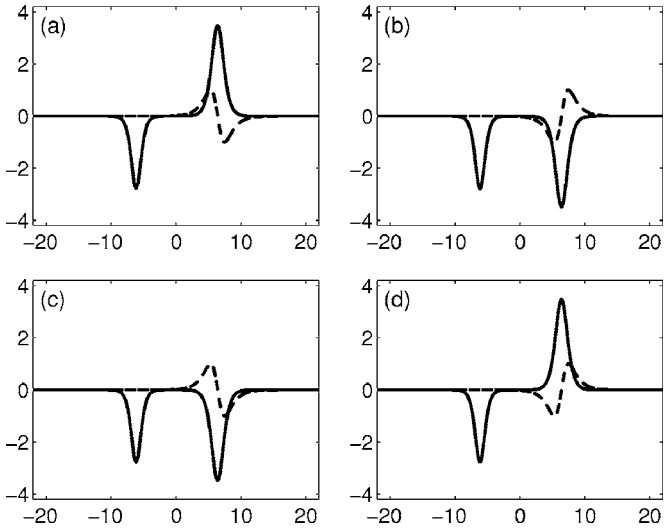

FIG. 3. The eigenfunctions of the bubble involving the right-handed [$\sigma=-1$, (a,b)] and left-handed [$\sigma=+1$, (c,d)] Bloch wall. These are obtained by numerically solving Eq. (12). The eigenfunction in (a,c) is associated with the positive and that in (b,d) with the negative eigenvalue. In this figure, $s=5$ and $h=0.2$. The real part is shown by the solid line, while the imaginary part is dashed.

simulations are presented in the next two sections, concurrently with predictions of the asymptotic analysis.

IV. INTERPRETATION OF THE EIGENFUNCTION

The eigenfunction associated with the eigenvalue $\lambda>0$ admits interpretation in terms of the motions of the constituent walls. Let, for definiteness, $s>0$ and $\sigma=-1$, and note that the dissociating bound state can be described by

$$\vec{\psi}(x,t) = \vec{\psi}_N(v_N(t);x+s+\delta s_N(t)-x^{(0)})+\cdots \tag{61a}$$

in the region $x<0$, and

$$\vec{\psi}(x,t) = \vec{\psi}_B(v_B(t);x-s-\delta s_B(t)-x^{(0)})+\cdots \tag{61b}$$

for $x>0$. Here $\vec{\psi}_N(v;x)$ and $\vec{\psi}_B(v;x)$ are stationary solutions of Eq. (7) with small v obtained by continuation from $\vec{\psi}_N(x)$ and $\vec{\psi}_B(x)$, respectively, and "$\cdots$" includes the part of the perturbation which cannot be reduced to the translation and velocity boost of the corresponding wall. Note that since we have not specified this part, the parameters v_N, v_B, δs_N, and δs_B are not defined uniquely in Eq. (61a); to fix these parameters we need to restrict the "$\cdots$" part in some way. To do this, we note that Eq. (61a) can be represented as $\vec{\psi}_b(x)+\delta\vec{\psi}(x,t)$, where $\vec{\psi}_b(x)=(\mathcal{R},\mathcal{I})$ is the stationary bubble Eq. (11) with some s and $x^{(0)}$, and a small perturbation $\delta\vec{\psi}(x,t)$ can be written in the form

$$\delta\vec{\psi}(x,t) = v_N(t)\dot{\vec{\psi}}_N+\delta s_N(t)\vec{\psi}'_N+\vec{\nu}(x,t), \tag{62a}$$

$$\delta\vec{\psi}(x,t) = v_B(t)\dot{\vec{\psi}}_B-\delta s_B(t)\vec{\psi}'_B+\vec{\nu}(x,t) \tag{62b}$$

in $x<0$ and $x>0$, respectively. Here

$$\dot{\vec{\psi}}_N \equiv \partial_v\vec{\psi}_N(v;x+s-x^{(0)})|_{v=0};$$

$$\vec{\psi}'_N \equiv \partial_x\vec{\psi}_N(0;x+s-x^{(0)});$$

$$\dot{\vec{\psi}}_B \equiv \partial_v\vec{\psi}_B(v;x-s-x^{(0)})|_{v=0};$$

$$\vec{\psi}'_B \equiv \partial_x\vec{\psi}_B(0;x-s-x^{(0)}).$$

(We remind that the overdot stands for the partial derivative with respect to v, not t, here.) For the given s and $x^{(0)}$, we can fix v_N, v_B, δs_N, and δs_B by requiring that the "remainder" $\vec{\nu}(x,t)$ be J-orthogonal to the subspace spanned by the velocity boosts and translations:

$$\int_{-\infty}^{0}\langle\vec{\nu},J\dot{\vec{\psi}}_N\rangle dx=\int_{-\infty}^{0}\langle\vec{\nu},J\vec{\psi}'_N\rangle dx=0, \tag{63a}$$

$$\int_{0}^{\infty}\langle\vec{\nu},J\dot{\vec{\psi}}_B\rangle dx=\int_{0}^{\infty}\langle\vec{\nu},J\vec{\psi}'_B\rangle dx=0. \tag{63b}$$

Here $\langle,\rangle$ denotes the scalar product in the two-dimensional Euclidean space: $\langle\vec{f},\vec{g}\rangle\equiv f_1g_1+f_2g_2$. From Eq. (63a) we have

$$v_N=\frac{(\delta\vec{\psi},J\vec{\psi}'_N)}{(\dot{\vec{\psi}}_N,J\vec{\psi}'_N)}$$

and similar expressions for v_B, δs_N, and δs_B. One more consequence of the constraints Eq. (63a) is that $\vec{\nu}(x,t)$ is linearly independent from $\dot{\vec{\psi}}_N$ and $\vec{\psi}'_N$ in the region $x<0$ and from $\dot{\vec{\psi}}_B$ and $\vec{\psi}'_B$ in the region $x>0$. [Indeed, if we assumed $\vec{\nu}=c_1\vec{\psi}'_N+c_2\dot{\vec{\psi}}_N$ and substituted this in Eq. (63a), then using the fact that $(\vec{\psi}'_N,J\dot{\vec{\psi}}_N)=\frac{1}{2}\dot{P}_N\neq0$, we would immediately get $c_1=c_2=0$.]

The perturbation Eq. (62a) can be expanded over solutions of the equation (12):

$$\begin{aligned}\delta\vec{\psi}=&\mathcal{M}_ue^{\lambda t}\vec{\varphi}_u+\mathcal{M}_se^{-\lambda t}\vec{\varphi}_s\\&+\mathcal{N}_0\vec{\psi}'_b+\tilde{\mathcal{N}}_0\partial_s\vec{\psi}_b+\mathcal{Q}^{(+)}e^{i\omega_0t}\vec{\phi}^{(+)}+\mathcal{Q}^{(-)}e^{-i\omega_0t}\vec{\phi}^{(-)}\\&+\int_{-\infty}^{\infty}\mathcal{Q}^{(1)}(k)e^{i\omega t}\vec{\phi}^{(1)}_k dk\\&+\int_{-\infty}^{\infty}\mathcal{Q}^{(2)}(k)e^{i\omega t}\vec{\phi}^{(2)}_k dk.\end{aligned} \tag{64}$$

In Eq. (64), $\vec{\varphi}_u$ and $\vec{\varphi}_s$ are the eigenfunctions associated with discrete real eigenvalues λ and $-\lambda$, respectively, where we set $\lambda>0$; $\vec{\psi}'_b$ and $\partial_s\vec{\psi}_b$ are the two zero modes while $\vec{\phi}^{(+)}$ and $\vec{\phi}^{(-)}$ are eigenfunctions associated with pure imaginary discrete eigenvalues $\pm i\omega_0$. Finally, $\vec{\phi}^{(1)}_k$ and $\vec{\phi}^{(2)}_k$ are solutions of the continuous spectrum, $\mathcal{H}\vec{\phi}^{(1,2)}_k=i\omega J\vec{\phi}^{(1,2)}_k$, with $\omega^2=\frac{1}{4}(k^2+4)(k^2+B^2)$, and $\omega(k)>0$ for $k>0$ and $\omega(k)<0$ for $k<0$.

As t grows, the expansion (64) tends to $\mathcal{M}_ue^{\lambda t}\vec{\varphi}_u$, where $\vec{\varphi}_u(x)$ is given by Eq. (60a). This should be identified with the large-t behavior of Eq. (62a). Using linear independence of vectors $\vec{\psi}'_N$, $\dot{\vec{\psi}}_N$, $\vec{\nu}$ in $x<0$ and vectors $\vec{\psi}'_B$, $\dot{\vec{\psi}}_B$, $\vec{\nu}$ in $x>0$, we get

$$\begin{aligned}v_N(t)&\to-\lambda\mathcal{M}_u\sqrt{\dot{P}_B}e^{\lambda t},\\v_B(t)&\to-\lambda\mathcal{M}_u\sqrt{-\dot{P}_N}e^{\lambda t};\end{aligned} \tag{65}$$

$$\begin{aligned}\delta s_N(t)&\to\mathcal{M}_u\sqrt{\dot{P}_B}e^{\lambda t},\\\delta s_B(t)&\to-\mathcal{M}_u\sqrt{-\dot{P}_N}e^{\lambda t}\end{aligned} \tag{66}$$

as $t\to\infty$. Equations (65) and (66) are consistent in the sense that the velocity of the wall determined from the deformation of its shape coincides with the velocity defined by the position of its center:

$$v_N(t)\to-\frac{d}{dt}\delta s_N(t),\quad v_B(t)\to\frac{d}{dt}\delta s_B(t).$$

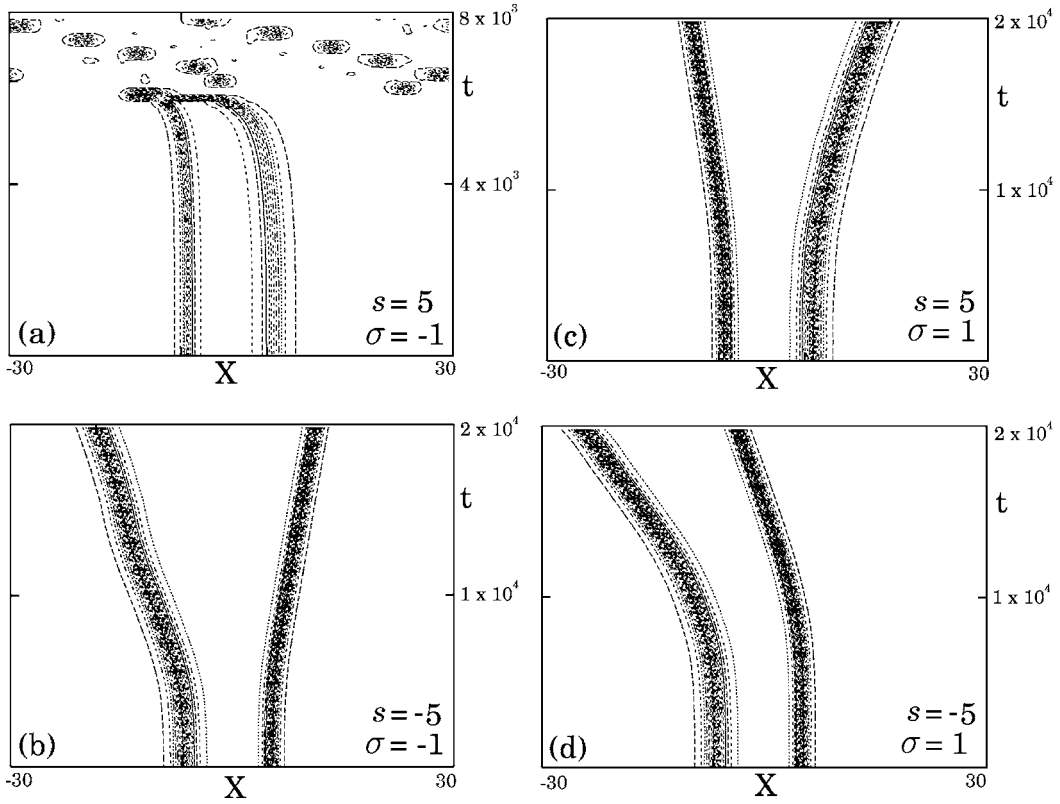

FIG. 4. The development of the instability of the bubble Eq. (11). Shown are the curves of constant real part. The wide and narrow trails pertain to the Bloch and Néel walls, respectively. Panels (a) and (b) correspond to bound states involving right-handed Bloch walls ($\sigma=-1$), with $s=5$ and $s=-5$, respectively. The evolution of the bubbles with the left-handed Bloch walls ($\sigma=+1$) is depicted in panels (c) and (d), also with $s=5$ and $s=-5$, respectively. No perturbations were added to the stationary initial condition (11) "by hand;" the initial (uncontrollable) disturbance was merely due to the discretization of the equation. The collision of two walls in (a) produces a breather. This breather moves so quickly that the contour plot seems to indicate the presence of two separate breathers whereas there is in fact only one. This effect is due to a sparse time-sampling of the profile which we had to resort to for better visualization. The image in (a) has been generated by saving a profile once only every 200 time units. In these plots, $h=0.1$.

Note that the derivative $\dot{P}_N$ is greater, in absolute value, than $\dot{P}_B$ (see Fig. 1). Consequently, Eq. (65) implies that the Bloch wall arising from the dissociation of the bubble, always moves faster than the emerging Néel wall: $|v_B|>|v_N|$. The same Eq. (65) implies that the corresponding velocities and accelerations of the Bloch and Néel walls will be colinear. Consequently, the walls emerging from the decay of the bubble with $s>0$ and $\sigma=-1$ will be moving in the same direction. (The direction will of course be determined by the initial perturbation.) This conclusion is in agreement with direct numerical simulations of Eq. (4). [See Fig. 4(a).]

It follows then from Eq. (65) that if $\mathcal{M}_u>0$, the two walls will be moving to the left, with the Bloch wall catching up with the Néel wall. This was indeed seen in simulations [Fig. 4(a)]. (In our numerical simulations, the choice $\mathcal{M}_u>0$ was accidental; the initial perturbation of the bubble was entirely due to the discretization errors and hence beyond our control.) On the contrary, if $\mathcal{M}_u<0$, the walls will be moving to the right, with the Néel wall lagging behind.

Changing $\sigma\to-\sigma$ swaps around the top components of the eigenfunction $\vec{\varphi}_u$ associated with $\lambda>0$ and eigenfunction $\vec{\varphi}_s$ pertaining to the negative eigenvalue $-\lambda$. Therefore the "unstable" eigenfunction of the bubble with $\sigma=+1$ involves coefficients a and b of the *opposite* signs. As a result, the fragments of its decay—the Néel and left-handed Bloch wall—will be moving in opposite directions. The simulations confirm this [Fig. 4(c)].

As we have already mentioned, the choice of the coefficient $\mathcal{M}_u$ was beyond our control in the simulations. For $s=5$ and $\sigma=+1$, our discretization induced $\mathcal{M}_u>0$. However, for a slightly different value of s, viz. $s=4.9$, the "unstable" eigenfunction $\vec{\varphi}_u$ was seen to be excited with the coefficient $\mathcal{M}_u<0$ (Fig. 5).

The effect of the change $s\to-s$ amounts to changing $\sigma\to-\sigma$ and $x\to-x$; therefore the dissociating bound state of the right-handed Bloch wall on the left of the Néel wall will produce walls moving in opposite directions. [Simulation shown in Fig. 4(b).] Finally, a left-handed Bloch wall ($\sigma=+1$) and a Néel wall placed on its right (i.e., $s<0$) will move in the same direction. If (as it happened in our simulations) $\mathcal{M}_u$ is >0, the Bloch will be leaving the Néel wall behind [Fig. 4(d)].

In the case of converging walls, the result of the collision in all cases is the formation of a spatially localized, temporally oscillating object (which we refer to as a breather), propagating over the constant background $\psi=1$. An asymptotic expression for the breather was derived in Ref.

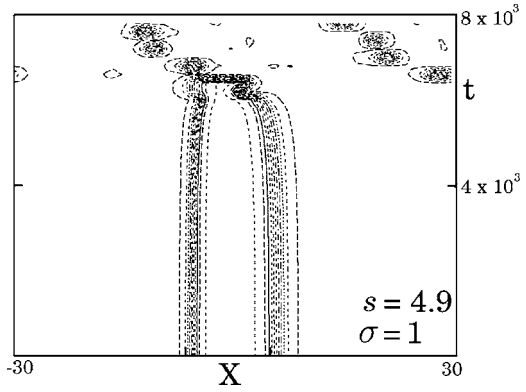

FIG. 5. Evolution of the bound state involving a left-handed Bloch wall ($\sigma=+1$), with $s=4.9$. This initial condition is almost identical to the initial condition that led to Fig. 4(c); however, the direction of motion of the walls is now exactly opposite. The reason, of course, is that $\mathcal{M}_u$ was positive in the perturbation of Fig. 4(c), whereas here, the "unstable" eigenfunction $\vec{\varphi}_u$ is excited with a negative coefficient. As in Fig. 4, in this plot $h=0.1$.

[1]; here, we simply note that it persisted indefinitely after it was formed in our simulations.

V. THE BLOCH-NÉEL INTERACTION

A. The method

Our knowledge of the phase space in the vicinity of the unstable bound state of the Bloch and Néel walls can be used to make conclusions on the evolution of particular initial configurations of the two walls. Any initial condition comprising well-separated Bloch and Néel walls can be represented as

$$\psi(x,0) = \psi_b(x) + \delta\psi(x,0),$$

where $\psi_b(x)$ is the bubble Eq. (11) with some suitably chosen separation s, centered at some point $x^{(0)}$, and $\delta\psi(x,0)$ is a small perturbation. This initial perturbation can be expanded as in Eq. (64) where we just need to set $t=0$. In order to find the coefficient $\mathcal{M}_u$ with which the unstable eigenvector $\vec{\varphi}_u$ enters the perturbation, we note that the J-product of the vector $\vec{\varphi}_s$ with any solution of Eq. (12) except $\vec{\varphi}_u$ is zero:

$$(\vec{\varphi}_s, J\vec{\varphi}_s) = (\vec{\varphi}_s, J\vec{\psi}_b{}') = (\vec{\varphi}_s, J\partial_s\vec{\psi}_b)$$
$$= (\vec{\varphi}_s, J\vec{\phi}^{(\pm)}) = (\vec{\varphi}_s, J\vec{\phi}_k^{(1)}) = (\vec{\varphi}_s, J\vec{\phi}_k^{(2)}) = 0.$$

[This is a simple consequence of the Hermiticity of the operator $\mathcal{H}$ in Eq. (12): if $\mathcal{H}\vec{\zeta}_1=\lambda_1 J\vec{\zeta}_1$ and $\mathcal{H}\vec{\zeta}_2=\lambda_2 J\vec{\zeta}_2$, then $(\lambda_1+\lambda_2)(\vec{\zeta}_1, J\vec{\zeta}_2)=0$. Hence $(\vec{\zeta}_1, J\vec{\zeta}_2)=0$ unless $\lambda_1=-\lambda_2$.] Therefore

$$\mathcal{M}_u = \frac{(\vec{\varphi}_s, J\delta\vec{\psi})}{(\vec{\varphi}_s, J\vec{\varphi}_u)}. \tag{67}$$

The sign of $\mathcal{M}_u$ determines the direction of colinear motion of the two walls. In fact, the denominator in Eq. (67) is positive and the sign of $\mathcal{M}_u$ is determined just by the sign of $(\vec{\varphi}_s, J\delta\vec{\psi})$. Indeed, using the representation (60a) for $\vec{\varphi}_s(x)$, $\vec{\varphi}_u(x)$ and invoking the identity (50), one can check that the integral over the negative semiaxis is zero to the leading order in ε:

$$\int_{-\infty}^{0} \langle \vec{\varphi}_s, J\vec{\varphi}_u\rangle dx = O(\varepsilon^2).$$

We remind that $\langle,\rangle$ is the scalar product in the two-dimensional Euclidean space: $\langle \vec{f}, \vec{g}\rangle \equiv f_1 g_1 + f_2 g_2$ whereas $(,)$ stands for the L^2-scalar product: $(\vec{f}(x), \vec{g}(x)) = \int_{-\infty}^{\infty} \langle \vec{f}, \vec{g}\rangle dx$. On the other hand, using the expansion (60b) for $0<x<\infty$, we obtain

$$\int_{0}^{\infty} \langle \vec{\varphi}_s, J\vec{\varphi}_u\rangle dx = -\lambda \dot{P}_N \dot{P}_B,$$

which is positive for $\lambda>0$ (see Fig. 1). Thus $(\vec{\varphi}_s, J\vec{\varphi}_u) = -\lambda\dot{P}_N\dot{P}_B + O(\varepsilon^2) > 0$. Q.E.D.

B. Example

As a characteristic example, we consider the initial condition of the form

$$\psi(x,0) = -\psi_N(x+x_1)\psi_B(x-x_1) \tag{68}$$

with some $x_1>0$. In applications, this product function is often used as an approximation for two well-separated dark solitons, in the same way as two weakly overlapping bright solitons are usually approximated by their sum. (See e.g., Ref. [1] where this type of ansatz was employed for the variational analysis of the Néel-Néel and Bloch-Bloch interactions.) Assuming that the Bloch wall is right-handed and that x_1 is large, we have

$$\text{Re}\ \psi(x,0) = -\tanh\xi + 2e^{2B(\xi-2x_1)}\tanh\xi + \cdots,$$

$$\text{Im}\ \psi(x,0) = 2\,\text{sech}\beta\, e^{B(\xi-2x_1)}\tanh\xi + \cdots \tag{69a}$$

in the region $x<0$, and

$$\text{Re}\ \psi(x,0) = \tanh(B\eta-\beta) - 2e^{-2(\eta+2x_1-\beta/B)}\tanh(B\eta-\beta) + \cdots,$$

$$\text{Im}\ \psi(x,0) = \text{sech}\beta\,\text{sech}(B\eta-\beta) - 2\,\text{sech}\beta\, e^{-2(\eta+2x_1-\beta/B)}\,\text{sech}(B\eta-\beta) + \cdots \tag{69b}$$

in the region $x>0$. Here we have defined ξ and η according to

$$\xi = x + x_1, \quad \eta = x - x_1 + \frac{\beta}{B}. \tag{70}$$

Note that the leading, $O(\varepsilon^0)$, terms in Eq. (69a) coincide, formally, with the leading terms in the asymptotic expansions of the bubble, Eqs. (15) and (29). However, the definitions of ξ and η in Eq. (70) will not, in general, be consistent with the definitions of ξ and η for the bubble, i.e., Eqs. (16)

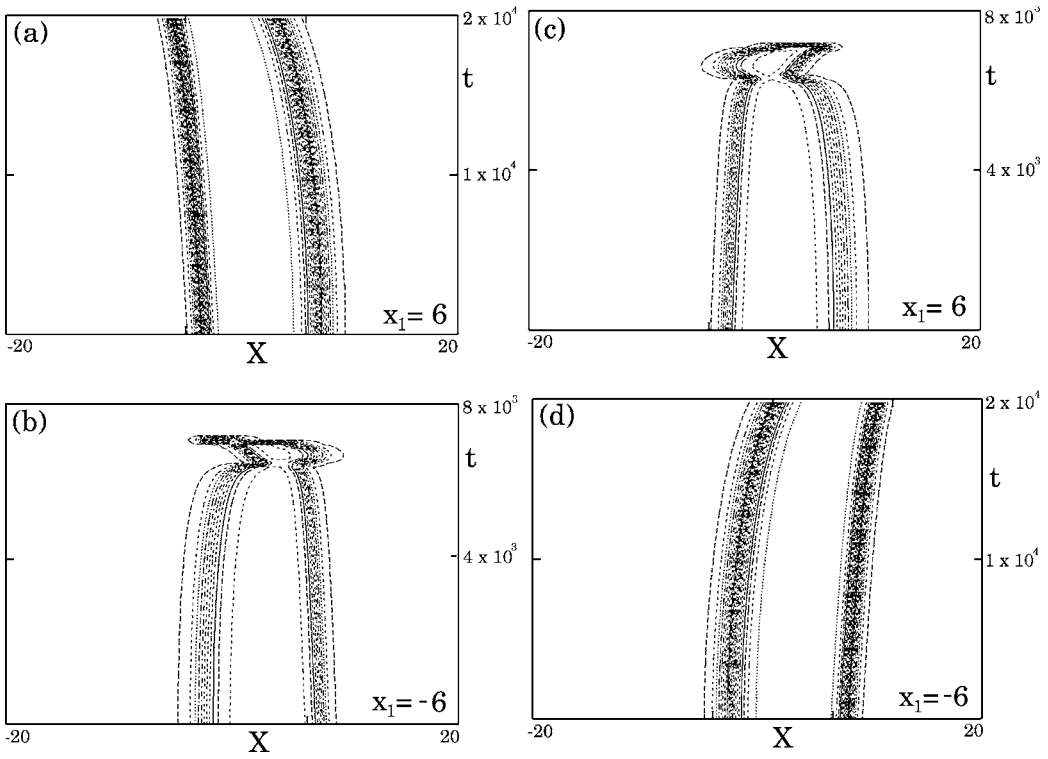

FIG. 6. Typical results of the evolution of an initial condition of the form (68). Panels (a) and (b) correspond to the *right*-handed Bloch wall, to the right ($x_1>0$) and the left ($x_1<0$) of the Néel wall, respectively. Panels (c) and (d) correspond to the *left*-handed Bloch wall, to the right and the left of the Néel wall, respectively. The Bloch wall moves towards the Néel wall in all cases. The Néel wall moves towards or away from the Bloch wall depending on whether it is on the left or right of the Bloch wall, and on the Bloch wall's chirality. After the collisions in (b) and (c), a fast-moving breather is formed; however, for visual clarity, this solution is not shown. Here, $h=0.1$.

and (30). To achieve the consistency, we introduce an additional translation parameter $x^{(0)}$ in the definitions (16) and (30):

$$\xi = x - x^{(0)} + s + \beta, \quad \eta = x - x^{(0)} - s. \tag{71}$$

Thus we allow for translations of the bubble to ensure the coincidence of the leading terms in Eqs. (69) with those in Eqs. (15) and (29). Equating Eq. (70) with (71) we obtain parameters of such a reference bubble:

$$s = x_1 - \frac{\beta}{2}\left(1 + \frac{1}{B}\right), \quad x^{(0)} = \frac{\beta}{2}\left(1 - \frac{1}{B}\right). \tag{72}$$

Subtracting the bubble solution with parameters (72) from the initial condition (68), we obtain the following expressions for $\mathrm{Re}\,\delta\psi \equiv \mathrm{Re}\,\psi(x,0) - \mathcal{R}(x)$ and $\mathrm{Im}\,\delta\psi \equiv \mathrm{Im}\,\psi(x,0) - \mathcal{I}(x)$:

$$\mathrm{Re}\,\delta\psi(x) = \varepsilon^2 e^{-2B\beta}\sinh(2\beta)\frac{e^{2(B-1)\xi}}{\cosh^2\xi} + \cdots,$$

$$\mathrm{Im}\,\delta\psi(x) = 2\varepsilon B e^{-B\beta}\frac{e^{(B-1)\xi}}{\cosh\xi} + \cdots \tag{73a}$$

in the region $x<0$, and

$$\mathrm{Re}\,\delta\psi(x) = \mu e^{-2\beta}\sinh(2\beta)\frac{e^{2(B-1)\eta}}{\cosh^2(B\eta-\beta)} + \cdots,$$

$$\mathrm{Im}\,\delta\psi(x) = 2\mu e^{-2\eta}\frac{\cosh(B\eta) - e^{-2\beta}\,\mathrm{sech}\,\beta\cosh(B\eta-\beta)}{\cosh^2(B\eta-\beta)} + \cdots \tag{73b}$$

for $x>0$. Here $\varepsilon = e^{-2Bs}$ and $\mu = e^{-4s}$; $\mathcal{R}$ and $\mathcal{I}$ are the real and imaginary parts of the solution Eq. (11): $\psi_b = \mathcal{R} + i\mathcal{I}$.

In order to evaluate the integral $(\vec{\varphi}_s, J\delta\vec{\psi})$ in Eq. (67), we note that the positive semiaxis of x gives a contribution of the order $e^{-(2+B)s}$. This is exponentially smaller than the contribution of the negative semiaxis (which is of the order e^{-2Bs}) and hence can be neglected. Using Eqs. (60a) and (73a) we then get

$$(\vec{\varphi}_s, J\delta\vec{\psi}) = 2\varepsilon\sqrt{-\dot{P}_N}\,B e^{-B\beta}\int_{-\infty}^{\infty} e^{(B-1)\xi}\,\mathrm{sech}^3\xi\,d\xi + \cdots$$

which is positive. Hence $\mathcal{M}_u>0$, and, according to Eqs. (65) and (66), both walls will be moving to the left.

The direct numerical simulations of Eq. (4) verify these conclusions. Figure 6 presents simulations of the initial condition (68) with $x_1=\pm 6$ and $h=0.1$, for both chiralities of the Bloch wall. (These results are representative of all h provided $|x_1|$ is sufficiently large.) When the Bloch wall is right-handed and x_1 is positive, i.e., when the Bloch wall is on the right of the Néel, both walls move to the left [Fig. 6(a)], precisely as our analysis predicted. Using symmetries of the initial condition (68) and the partial differential equation (4),

one can readily check that the evolutions shown in Figs. 6(b)–6(d) are in agreement with the asymptotic analysis as well.

VI. CONCLUDING REMARKS

A. Energy considerations

Equation (4) is conservative, with the energy integral given by

$$E = \frac{1}{2}\int \left\{ |\psi_x|^2 + |\psi|^4 - \frac{2}{A^2}|\psi|^2 - \frac{h}{A^2}[\psi^2 + (\psi^*)^2] + 1 \right\} dx. \tag{74}$$

The bubbles, being time-independent solutions of Eq. (4), must render the functional (74) stationary: $\delta E = 0$. Since they depend on s smoothly, it follows that $dE/ds = 0$: the energy of the bound state is independent of the distance between its constituents. This seems to suggest that the binding energy of the Bloch and Néel walls is zero, implying the noninteraction of the walls.

However, our analysis has revealed that the walls do, in fact, interact. We have shown that all bound states with the parameter $s \neq 0$ are exponentially unstable against the decay into constituent walls. Exponential growth of the intersoliton separation [see Eq. (66)] is a clear manifestation of a nonvanishing interaction between the walls—for noninteracting walls, the separation would only grow linearly. As for the zero binding energy, it can be reconciled with the nonvanishing interaction by noticing that the bound Néel wall acquires a small static imaginary part [see Eq. (15)]. (The bound Bloch wall also acquires a stationary perturbation, but it is exponentially smaller than the perturbation of the Néel wall.) To leading order, the force between two walls is made up of the force between their real parts and the force between their imaginary parts while the force between the real part of one wall and the imaginary part of the other one is of the second order of smallness [19]. The imaginary part of any nontrivial stationary solution decays as $O(e^{-Bx})$, while the real part decays as $O(e^{-2Bx})$ or $O(e^{-2x})$. Consequently, the force caused by the overlap of the imaginary parts of the soliton tails has a longer range than the force caused by overlapping real parts. Thus although the amplitude of the imaginary excitation of the Néel wall is exponentially small for large s, the interaction of this excitation with (the imaginary part of) the Bloch wall is enough to balance the force between the Bloch wall and the "naked" Néel wall. If we decrease s, and the two walls in the complex are pulled closer, the increase of (the absolute value of) the binding energy of their real parts is offset by storing more energy of the opposite sign in the imaginary excitations; the total energy remains invariant. A similar mechanism was described by Ostrovskaya *et al.* in the context of the dark-bright solitons of the undriven vector nonlinear Schrödinger equation [20]; there the imaginary excitations were referred to as "solitonic gluons."

B. Walls as particles

Next, we need to explain, qualitatively, the anomalous behavior apparent in Figs. 4(a), 4(d), 6(a), and 6(d), where the velocities and accelerations of the two interacting walls are seen to have the same (rather than the opposite) directions. The key observation here is that the Bloch and Néel walls, considered as pointlike particles, have masses of opposite signs (see Fig. 1). One can easily conceive a simple model system of positive- and negative-mass particles, which exhibits the observed phenomenology. Let x_1 and x_2 be the coordinates of the two particles, with $z \equiv x_1 - x_2$, and let $m_1 > 0$ and $m_2 < 0$ be their masses. Consider the Hamiltonian

$$H = \frac{1}{2m_1}(p_1 - f_1)^2 + \frac{1}{2m_2}(p_2 - f_2)^2, \tag{75}$$

where p_1, p_2 are the momenta of the particles, and the functions $f_1 = f_1(z)$ and $f_2 = f_2(z)$ decay, exponentially, as $|z| \to \infty$. The equations of motion are

$$\dot{p}_1 = -\frac{\partial H}{\partial x_1} = \frac{1}{m_1}(p_1 - f_1)f_1' + \frac{1}{m_2}(p_2 - f_2)f_2', \tag{76a}$$

$$\dot{p}_2 = -\frac{\partial H}{\partial x_2} = -\dot{p}_1, \tag{76b}$$

$$\dot{x}_1 = \frac{\partial H}{\partial p_1} = \frac{1}{m_1}(p_1 - f_1), \tag{76c}$$

$$\dot{x}_2 = \frac{\partial H}{\partial p_2} = \frac{1}{m_2}(p_2 - f_2), \tag{76d}$$

where the overdot indicates differentiation with respect to time, t (and not v as earlier in the text). The prime stands for the derivative with respect to z.

For any $z = z_0$, Eqs. (76) have a fixed point, describing an unstable bound state of two particles:

$$p_1 = f_1(z_0), \quad p_2 = f_2(z_0). \tag{77}$$

This fixed point is an analog of the bound state of two walls, Eq. (11). Linearizing Eqs. (76) about the equilibrium point (77), and letting $\delta p_{1,2}(t), \delta x_{1,2}(t) \propto e^{\lambda t}$, we get a pair of nonzero real eigenvalues

$$\lambda^{(\pm)} = \pm \frac{1}{\sqrt{-m_1 m_2}}[f_1'(z_0) + f_2'(z_0)]. \tag{78}$$

(There is also a pair of *zero* eigenvalues resulting from the overall translations $x_{1,2} \to x_{1,2} - x^{(0)}$ and the freedom in choosing z_0.) Working out the associated eigenvectors and substituting them into the linearized equations (76c) and (76d), we find

$$m_1 \delta\dot{x}_1 = \pm \frac{K^{(\pm)}}{\sqrt{|m_2|}}\delta z, \tag{79a}$$

$$|m_2|\,\delta\dot{x}_2 = \frac{K^{(\pm)}}{\sqrt{m_1}}\delta z, \tag{79b}$$

where $K^{(\pm)}$ are coefficients dependent on $m_{1,2}$ and $f_{1,2}'(z_0)$.

If $f_1'(z_0) + f_2'(z_0) > 0$, the unstable eigenvalue is $\lambda^{(+)}$, and we keep the top sign in Eq. (79a). This is the case of anoma-

lous behavior: the velocities $\delta\dot{x}_1$ and $\delta\dot{x}_2$ as well as accelerations $\delta\ddot{x}_1$ and $\delta\ddot{x}_2$ have the same sign and so the particles move in the same direction, like the walls in Figs. 4(a), 4(d), 6(a), and 6(d). If $f_1'(z_0)+f_2'(z_0)<0$, the positive eigenvalue is $\lambda^{(-)}$ and the "unstable" eigenvector is given by Eq. (79a) with the bottom sign. In this case the two particles have opposite velocities and opposite accelerations; this corresponds to the "normal" interaction of the Bloch and Néel wall seen in panels (b) and (c) of Figs. 4 and 6. (It is fitting to note here that the anomalous behavior does not mean that the two particles violate the third Newton's law. The force exerted by the particle 2 on particle 1, $-\partial H/\partial x_1$, is exactly opposite to the back reaction force, $-\partial H/\partial x_2$.)

C. Conclusions

Finally, we summarize the results of this investigation. The essence of our approach is to consider the interacting Bloch and Néel walls as a perturbation of their unstable stationary complex. The interaction between the two walls is characterized by the eigenfunction associated with the positive eigenvalue in the spectrum of the linearized operator (evaluated at this stationary solution).

Using matched asymptotic expansions, we have evaluated the real eigenvalues for the Bloch-Néel complex and constructed the associated eigenfunctions. The structure of the "unstable" eigenfunction for the complex consisting of a right-handed Bloch wall on the right, and a Néel wall on the left, indicates that the walls emerging from the decay of this "bubble," will be moving colinearly, i.e., in the same direction. This rule determines the evolution of a general configuration of a right-handed Bloch wall on the right and a Néel wall on the left—as long as the walls are sufficiently far away from each other. Using symmetry properties of the Bloch-Néel complex, we can also predict the type of motion (colinear or antilinear) for other chiralities and mutual arrangements of the walls. The asymptotic analysis is in agreement with direct numerical simulations of the interacting Bloch and Néel walls.

Although the unstable eigenfunction determines the type of motion of two interacting walls, knowing the structure of this eigenfunction is insufficient to know which direction this motion will take. (Depending on whether the unstable eigenfunction is excited with a positive or negative coefficient, the colinearly moving walls may travel to the left or to the right. Similarly, in those cases where the unstable eigenfunction sets the opposite direction of motion for the walls, they may travel either towards or away from each other.) The actual direction of the colinear or antilinear motion depends on the particular initial condition and can be determined by the projection of the corresponding perturbation of the stationary complex on its unstable eigendirection. We have evaluated this projection for an initial condition in the form of a product of the Bloch- and Néel-wall solutions, and verified the conclusions of the asymptotic analysis numerically. Finally, we have interpreted the anomalous interaction of the Bloch and Néel walls as a dynamics of two interacting particles, one with positive and the other with negative mass.

ACKNOWLEDGMENTS

It is a pleasure to thank Elena Zemlyanaya for testing, numerically, some aspects of the perturbation theory in Sec. III. We are grateful to Vladimir Gerdzhikov and Boris Malomed for useful discussions. One of the authors (I.B.) thanks Dr. Reinhard Richter and Professor Ingo Rehberg for their hospitality at the University of Bayreuth where this project was completed. I.B. is supported by the Ernest Oppenheimer Memorial Trust and also supported by the NRF of South Africa under Grant No. 2053723. S.W. was supported by the NRF of South Africa.

[1] I. V. Barashenkov, S. R. Woodford, and E. V. Zemlyanaya, Phys. Rev. E **74**, 026604 (2007).
[2] L. N. Bulaevskii and V. L. Ginzburg, Sov. Phys. JETP **18**, 530 (1964).
[3] R. Rajaraman and E. J. Weinberg, Phys. Rev. D **11**, 2950 (1975).
[4] J. Lajzerowicz and J. J. Niez, in *Solitons and Condensed Matter Physics*, edited by A. R. Bishop and T. Schneider, Springer Series in Solid-State Sciences Vol. 8 (Springer-Verlag, Berlin, 1978).
[5] J. Lajzerowicz and J. J. Niez, J. Phys. (Paris) **40**, L165 (1979).
[6] C. Elphick and E. Meron, Phys. Rev. A **40**, 3226 (1989).
[7] S. Sarker, S. E. Trullinger, and A. R. Bishop, Phys. Lett. **59**, 255 (1976).
[8] C. Montonen, Nucl. Phys. B **112**, 349 (1976).
[9] I. V. Barashenkov, S. R. Woodford, and E. V. Zemlyanaya, Phys. Rev. Lett. **90**, 054103 (2003).
[10] R. Rajaraman, Phys. Rev. Lett. **42**, 200 (1979).
[11] K. R. Subbaswamy and S. E. Trullinger, Physica D **2**, 379 (1981).
[12] P. Hawrylak, K. R. Subbaswamy, and S. E. Trullinger, Phys. Rev. D **29**, 1154 (1984).
[13] I. V. Barashenkov and S. R. Woodford, Phys. Rev. E **71**, 026613 (2005).
[14] I. V. Barashenkov and V. G. Makhankov, Phys. Lett. A **128**, 52 (1988); I. V. Barashenkov and E. Yu. Panova, Physica D **69**, 114 (1993).
[15] L. D. Landau and E. M. Lifshitz, *Quantum Mechanics*, 3rd ed. (Butterworth-Heinemann, Oxford, 1997), see problem 3 in Sec. 50, Chap. VII.
[16] I. V. Barashenkov, Phys. Rev. Lett. **77**, 1193 (1996).
[17] See Appendix A6 in V. I. Arnol'd, *Mathematical Methods of Classical Mechanics (Graduate Texts in Mathematics)* (Springer-Verlag, New York, 1989).
[18] J. A. C. Weideman and B. M. Herbst, SIAM (Soc. Ind. Appl. Math.) J. Numer. Anal. **23**, 485 (1986).
[19] B. A. Malomed and A. A. Nepomnyashchy, Europhys. Lett. **27**, 649 (1994).
[20] E. A. Ostrovskaya, Y. S. Kivshar, Z. G. Chen, and M. Segev, Opt. Lett. **24**, 327 (1999).